Acta Cryst. (1996). A**52**, 419–426

New Developments in Direct Shape Determination from Small-Angle Scattering. 2. Uniqueness

D. I. SVERGUN,[a,b]* V. V. VOLKOV,[b] M. B. KOZIN[b] AND H. B. STUHRMANN[c]

[a]*European Molecular Biology Laboratory, Hamburg Outstation, EMBL, c/o DESY, Notkestrasse 85, D-22603 Hamburg, Germany,* [b]*Institute of Crystallography, Russian Academy of Sciences, Leninsky prospekt 59, 117333 Moscow, Russia, and* [c]*GKSS Research Centre, GKSS-WS, D-21502 Geesthacht, Germany. E-mail: svergun@embl-hamburg.de*

(*Received 18 October 1995; accepted 2 January 1996*)

Abstract

The problem of uniqueness of the low-resolution shape determination from small-angle scattering by isotropic monodisperse systems is considered. The particle shape is represented by the envelope function parameterized using spherical harmonics as described in a previous paper [Svergun & Stuhrmann (1991). *Acta Cryst.* A**47**, 736–744]. Computer simulations are made on the model bodies with sharp boundaries exactly represented by spherical harmonics. If the number of independent parameters describing the shape is 1 to 1.5 times the number of Shannon channels covered by the data set, the shape restoration is found to be unique and stable with respect to the random and systematic errors. The resolution limits of the straightforward shape determination are connected to the computational accuracy of the model intensities; with current algorithms, shapes described by 15 to 20 independent parameters can be uniquely determined. The results form a basis for an *ab initio* low-resolution shape determination in terms of spherical harmonics.

1. Introduction

In low-resolution diffraction studies, homogeneous models often serve as a good approximation to the structure of the object. In particular, this is the case for small-angle scattering (SAS) studies of biological macromolecules in solution (Feigin & Svergun, 1987; Koch, 1991). The SAS intensity $I(s)$ from a dilute monodisperse system of dissolved particles is proportional to the scattering from a single particle averaged over all orientations [s denotes the modulus of the momentum transfer vector $\mathbf{s}$, $s = (4\pi/\lambda)\sin\theta$, λ is the wavelength and 2θ the scattering angle]. The spherical average leads to a significant loss of information in the scattering data which restricts the resolution to the range of about 2–10 nm. This justifies the interpretation of the SAS data in terms of the particle shape, which still provides valuable information about the quaternary structure of native biopolymers in solution.

Experimental data fitting using simple approximations like triaxial ellipsoids or more complicated models built from spheres (see *e.g.* Feigin & Svergun, 1987) is often used to describe the particle shape, the main problem being the construction of a model that fits the available data. In our previous paper (Svergun & Stuhrmann, 1991), we described changes to the direct shape determination method of Stuhrmann (1970*b*) that improve the fit to the scattering curves and proposed a strategy for low-resolution shape determination. The principal question that remains open in structural studies of biopolymers in solution is whether the low-resolution shape determination is unique, in other words, whether two shapes, being significantly different at low resolution, can yield scattering curves indistinguishable from each other within the experimental errors?

It is obvious that in the general case no unique solution exists as it is impossible to determine three-dimensional shape from one-dimensional intensity unambiguously. Granted that the information content in SAS is low, only a few parameters can be extracted from the scattering data; at low resolution, however, these may suffice to describe the particle shape adequately. If (i) the parameterization is general (that is, if any shape can be approximated by the chosen set of parameters at the given level of resolution) and if (ii) the parameters providing the best fit to the given scattering data can be uniquely determined and if (iii) their determination is stable with respect to the experimental errors, one can say that the low-resolution shape determination is unique.

A quantitative estimate of what 'a few parameters' actually means follows from Shannon's theorem (Shannon & Weaver, 1949; Moore, 1980; Taupin & Luzzati, 1982). The particle scattering intensity $I(s)$ is an analytical function that is completely defined by its values in the sampling points (Shannon channels) $I(s_k)$, $s_k = k\pi/D_{max}$, $k = 0, 1, \ldots, \infty$, where D_{max} is the maximum particle size. Thus, given the scattering curve in the interval $[s_{min}, s_{max}]$, the number of Shannon channels $N_s = (s_{max} - s_{min})D_{max}/\pi$ provides guidance on how many parameters can be extracted. At the same time, full information about the entire analytical function is

ISSN 0108-7673

Table 1. *R_ω factor of restoration of model shapes (in %)*

	Range *B*		Range *C*		Range *D*					
	Exact	Noisy	Exact	Noisy	Exact	Noisy		Quazi-real		
Model	data	data	data	data	data	data		conditions		
$L=3$	$N_s=2$		$N_s=4$		$N_s=6$			$N_s=6$		
	7.4	10.4	4.2	6.1	1.4	5.1	5.9	5.3	5.9	6.3
	9.9	33.0	0.2	5.0	0.5	1.4				
	11.1	27.1	7.9	44.0	5.4	10.2				
$L=4$	$N_s=3$		$N_s=7$		$N_s=13$			$N_s=13$		
	9.2	13.3	12.4	11.6	3.9	9.2	10.0	10.4	10.0	10.4
	10.7	17.2	8.3	25.3	3.8	10.0				

contained in any finite contiguous portion of it. A scattering curve measured with the angular increment much smaller than the sampling distance $\pi/D_{\max}$ can in principle be extrapolated beyond the experimental range [analytical continuation well known in optical image reconstruction, see *e.g.* Hunt (1994)], thus providing more than N_s independent parameters. The quality of the analytical extrapolation (and therefore of this additional information) depends on the experimental errors ranging from perfect extrapolation for error-free data to absurd extrapolations at high noise levels.

One can therefore expect that the models described by $N_I \cong N_s$ independent parameters can be uniquely determined. At low resolution, particle shape is conveniently parameterized using the envelope function of Stuhrmann (1970*b*). In this paper, we perform model calculations to study the uniqueness of the shape determination in terms of this parameterization.

2. Theory

A general model of the particle shape applicable to a wide variety of homogeneous particles at low resolution is given by the angular envelope function $F(\omega)$:

$$\rho(\mathbf{r}) = \begin{cases} 1, & 0 \le r \le F(\omega) \\ 0, & r \ge F(\omega), \end{cases} \tag{1}$$

where $\rho(\mathbf{r})$ is the scattering density, which equals 1 inside the particle and 0 elsewhere, and $(r, \omega) = (r, \theta, \varphi)$ are spherical coordinates. The envelope function is conveniently parameterized using the multipole expansion

$$F(\omega) \cong F_L(\omega) = \sum_{l=0}^{L} \sum_{m=-l}^{l} f_{lm} Y_{lm}(\omega), \tag{2}$$

where $Y_{lm}(\omega)$ are spherical harmonics and the multipole coefficients f_{lm} are complex numbers:

$$f_{lm} = \int_\omega F(\omega) Y^*_{lm}(\omega)\, \mathrm{d}\omega. \tag{3}$$

The spatial resolution of the shape representation (2) is defined by the truncation value L as $\delta \cong \pi R_0/(L+1)$, where R_0 is the radius of the equivalent sphere. Thus, the particle shape is parameterized by $(L+1)^2$ numbers and the accuracy of this representation increases with L due to the orthogonal properties of the spherical harmonics [$F_L(\omega) \to F(\omega)$ with $L \to \infty$].

Following Stuhrmann (1970*a*,*b*), the shape scattering intensity is expressed as

$$I(s) = \sum_{l=0}^{\infty} \sum_{m=-l}^{l} 2\pi^2 |A_{lm}(s)|^2, \tag{4}$$

where the partial amplitudes $A_{lm}(s)$ are represented by the power series

$$A_{lm}(s) = (is)^l (2/\pi)^{1/2} \sum_{p=0}^{p_{\max}} \Big((-1)^p f_{lm}^{(l+2p+3)} \times \{2^p p!(l+2p+3)[2(l+p)+1]!!\}^{-1} s^{2p} \Big) \tag{5}$$

and the coefficients of the qth power of the shape

$$f_{lm}^{(q)} = \int_\omega [F(\omega)]^q Y^*_{lm}(\omega)\, \mathrm{d}\omega \tag{6}$$

are readily evaluated from the f_{lm} values using the recurrence relation of Svergun & Stuhrmann (1991). Note that, although the series (4) is infinite, the contribution of the partial amplitudes with $l > L$ is relatively small.

3. Shape determination

Given the experimental scattering curve $I_{\exp}(s)$ specified for N points s_i, the shape determination can be performed by minimizing the least-squares deviation between $I_{\exp}(s)$ and $I(s)$:

$$R_I^2(I_{\exp}, f_{lm}) = \sum_{i=1}^{N} \{[I_{\exp}(s_i) - I(s_i)]^2 W(s_i)\} \times \left\{ \sum_{i=1}^{N} [I_{\exp}(s_i)^2 W(s_i)] \right\}^{-1}, \tag{7}$$

where $W(s)$ is a weighting function, *e.g.* $W(s_i) = \sigma^{-1}(s_i)$, where $\sigma(s_i)$ is the standard deviation in the ith

point. Starting from an initial shape described by the set of coefficients $f_{lm}^{(\mathrm{start})}$, the coefficients providing the best fit to $I_{\exp}(s)$ can be found by an iterative non-linear optimization procedure (see *e.g.* Gill, Murray & Wright, 1981).

A practical non-linear minimization requires both fast calculation of the functional (7) and an effective optimization algorithm. The details of the procedures improving the speed and accuracy of the evaluation of $I(s)$ from the given set of coefficients f_{lm} using (4)–(6) have been described elsewhere (Svergun & Stuhrmann, 1991; Svergun, 1994). For the minimization of (7), the software package *NL2SOL* was used based on the algorithm of Dennis, Gay & Welsch (1981). This algorithm utilizes the least-squares structure of the functional and proves to be much more effective than the general-purpose (*e.g.* gradient) methods. Application of *NL2SOL* significantly improved the convergence and allowed much better fits to the data [up to 4–6 orders of magnitude in the value of the functional (7) compared to the variable metrics methods we used earlier (Svergun & Stuhrmann, 1991)].

In all model calculations below, coefficients of the power series (5) up to $p_{\max} = 40$ (addition of extra terms did not improve the accuracy due to the rounding errors) were used to evaluate the rational Padé approximant as described by Svergun (1994), yielding an extended range of convergence over s. The intensity series (4) was truncated at $l = L + 5$, thus making the termination effects negligible. The functional to be minimized was

$$\Phi(I_{\exp}, f_{lm}) = R_I^2(I_{\exp}, f_{lm}) + \mu \mathbf{r}_0^2 + \nu H^2, \qquad (8)$$

where $\mathbf{r}_0$ and H are the coordinates of the geometrical center and the relative measure of negativity of $F(\omega)$, respectively. The first penalty term keeps the particle center close to the origin, the second ensures that $F(\omega)$ is positive definite (μ and ν are self-adjustable multipliers, both initially of order of 10^{-2}).

Our shape-determination program running on the Sparc-20ZX Sun workstation is coupled with the specially developed interactive three-dimensional solid rendering program *ASSA*. This allows one to monitor the fit to the experimental data and to follow the evolution

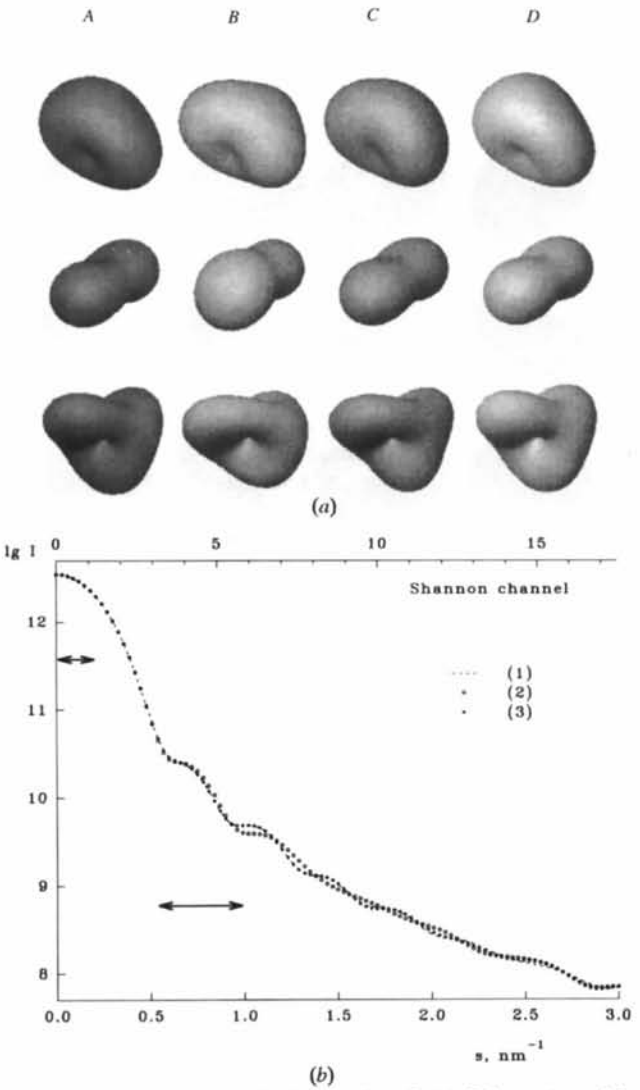

Fig. 1. Model-shape determination for $L = 3$. (*a*) Column *A*: model bodies. Columns *B*–*D*: results of the shape determination using the ideal $I(s)$ calculated from model bodies in the ranges [0, 0.2], [0.7, 1] and [0, 1] nm^{-1}, respectively. (*b*) Scattering from the bodies in the top row: curves (1)–(3) correspond to the bodies *A*–*C*, respectively; scattering from the body *D* is not distinguishable from that of model *A*. The double arrows indicate the angular ranges used to restore the bodies *B* and *C*. The top axis indicates the corresponding Shannon channels (in units of $sD_{\max}/\pi$, where $D_{\max} = 18.3$ nm is the maximum size of the model particles).

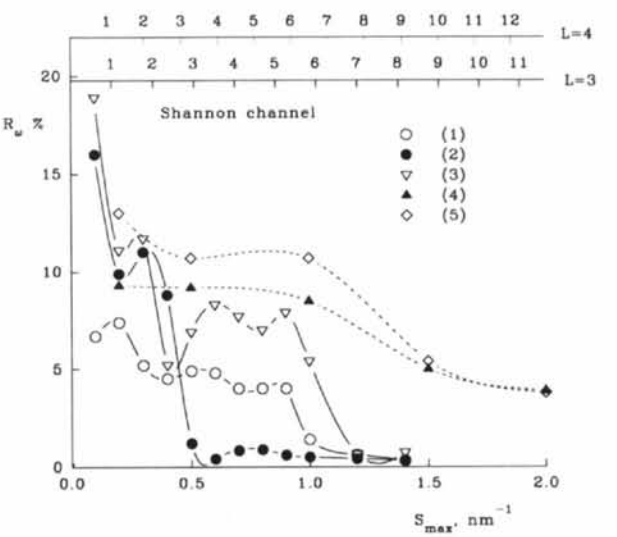

Fig. 2. R_ω factors of the shape restoration as functions of the angular range. (1)–(3) correspond to the restoration of different bodies at $L = 3$ (column *A* in Fig. 1*a*), (4)–(5) to the restoration of body *A* in Fig. 3(*a*) at $L = 4$ using two different initial approximations. Positions of the Shannon channels for $L = 3$ and 4 differ because of the different $D_{\max}$.

of the shape during minimization. *ASSA* was also used to produce the shaded models in the figures below.

4. Model calculations

The first series of model calculations was performed on error-free data. Continuous scattering curves were simulated by evaluating the scattering from models on $N = 100$ knots on finite intervals and the simulated data sets were used for the shape restoration. In the absence of experimental errors, the weighting function $W(s) = s^2$ was taken (Svergun & Stuhrmann, 1991).

Fig. 1(*a*) presents three model shapes generated with the spherical harmonics up to $L = 3$ (that is, each described by 16 parameters) and their restorations from different portions of the simulated scattering curves. In all cases, a sphere was used as the initial approximation. The first model (top row) represents a globular particle whereas the two others are rather anisometric. The scattering curve for the first model is displayed in Fig. 1(*b*) along with the scattering from the restored shapes. In this and subsequent figures, the scattering curves are presented also beyond the angular ranges used for the shape restoration to illustrate the analytical continuations. All the model shapes have the same maximum size $D_{max} = 18.3$ nm and the corresponding

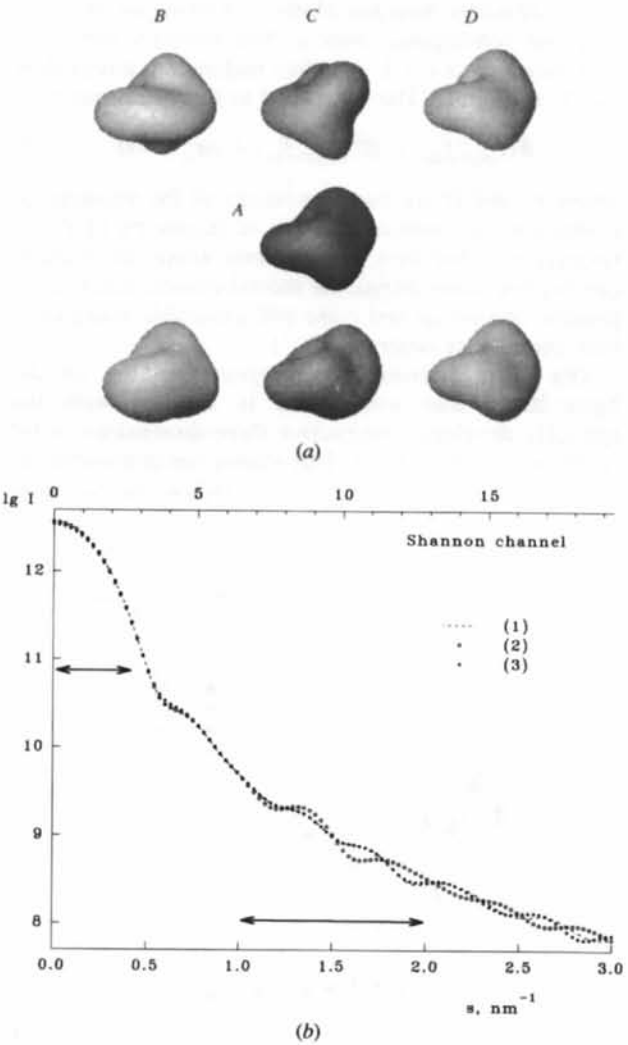

Fig. 3. Model-shape determination for $L = 4$. (*a*) Central body *A* represents the initial model, bodies *B*–*D* are obtained by restorations using the angular ranges [0, 0.5], [1, 2] and [0, 2] nm^{-1}, respectively, starting from a spherical initial approximation (top row) or an anisometric initial approximation (bottom row). (*b*) Corresponding scattering curves (notations are the same as in Fig. 1, curves from the restored models in the top row are presented, $D_{max} = 20.3$ nm).

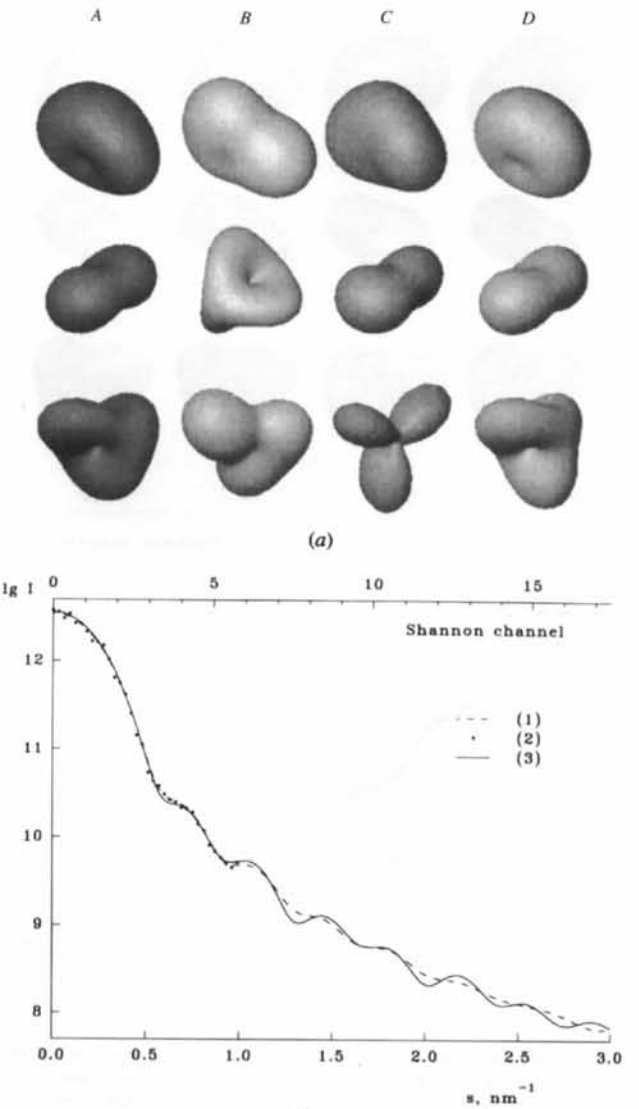

Fig. 4. Model-shape determination for $L = 3$ in the presence of random errors using the same angular ranges as in Fig. 1. (*a*) Model bodies and their restorations (notations are the same as in Fig. 1*a*). (*b*) Scattering from the bodies in the top row: (1) ideal scattering from the initial model *A*; (2) the same curve with 10% relative noise added; (3) scattering from the restored body *D*.

Shannon channels are indicated in the upper axis in Fig. 1(*b*). As the orientation of the restored shapes is arbitrary, for the comparison they are rotated to minimize the R_ω factor

$$R_\omega^2 = \int_\omega [F_{\text{model}}(\omega) - F_{\text{restored}}(\omega)]^2 \, d\omega \times \left\{ \int_\omega [F_{\text{model}}(\omega)]^2 \, d\omega \right\}^{-1}. \quad (9)$$

The surprisingly good restorations obtained even from very limited portions of the scattering curves (Table 1) indicate that the contributions from the low-order spherical harmonics are easily distinguishable in the scattering curve. It is worth noting that the R_ω factor is significantly improved when the number of Shannon channels N_s in the range used reaches the number of independent parameters in the model (Fig. 2). The latter [$N_I = (L+1)^2 - 6 = 10$] is smaller than the total number of parameters in (2), being reduced by six due to the arbitrary orientation of the particle and fixing its geometrical center at the origin.

In the simulations for the model structures up to $L = 4$ (19 independent parameters, $D_{\max} = 20.3$ nm), the shape restoration was performed starting from different initial approximations. The top row in Fig. 3(*a*) corresponds to the spherical initial approximation whereas the shapes in the bottom row were obtained starting from an anisometric shape with artificially enhanced contribution from higher harmonics. Increasing the number of parameters worsens the numerical stability of the algorithm, and therefore the use of restricted portions of the scattering curve (Fig. 3*b*) leads to higher R_ω factors than those for $L = 3$. However, extending the fitting range allows practically unambiguous shape restoration independent of the initial approximation [Table 1 and Fig. 3(*a*), column *D*].

To check the stability of the procedure with respect to random errors, Gaussian noise was added to the simulated scattering curves and the shape restoration was done using the error-containing data. Figs. 4 and 5 and Table 1 illustrate the results obtained on the same models and for the same angular ranges as above with a relative noise of 10% added. Use of limited portions of the scattering curves in the presence of noise, especially for $L = 4$, gives results that depend on the initial approximation and may deviate significantly from the models. At the same time, the full ranges (6 and 13 Shannon channels for $L = 3$ and $L = 4$, respectively) still ensure a reasonable restoration of the initial models in spite of the high level of random errors.

The example in Fig. 6 presents the restoration of the model shapes in quasi-real conditions: for both $L = 3$ and $L = 4$, the Guinier portions of the scattering curves were cut out, the Gaussian noise of 3% was generated and a constant (equal to the last intensity value) was added simulating the systematic deviations (Figs. 6*b*,*c*). In Fig. 6(*a*), four restorations for each model structure are given that differ by the initial approximation and by the random sequence taken to generate the noise. For $L = 3$, the solution is practically independent of these factors; for $L = 4$, minor variations are observed but the resulting shapes do not differ from the model body more than $R_\omega = 10.4\%$ (Table 1).

5. Limitations

The success of the shape restoration depends not only on the efficiency of the minimization technique but also on the computational accuracy in evaluating $I(s)$. Fig. 7 presents the relative error in the numerical evaluation of $I(s)$ according to (4)–(6) as a function of the number of

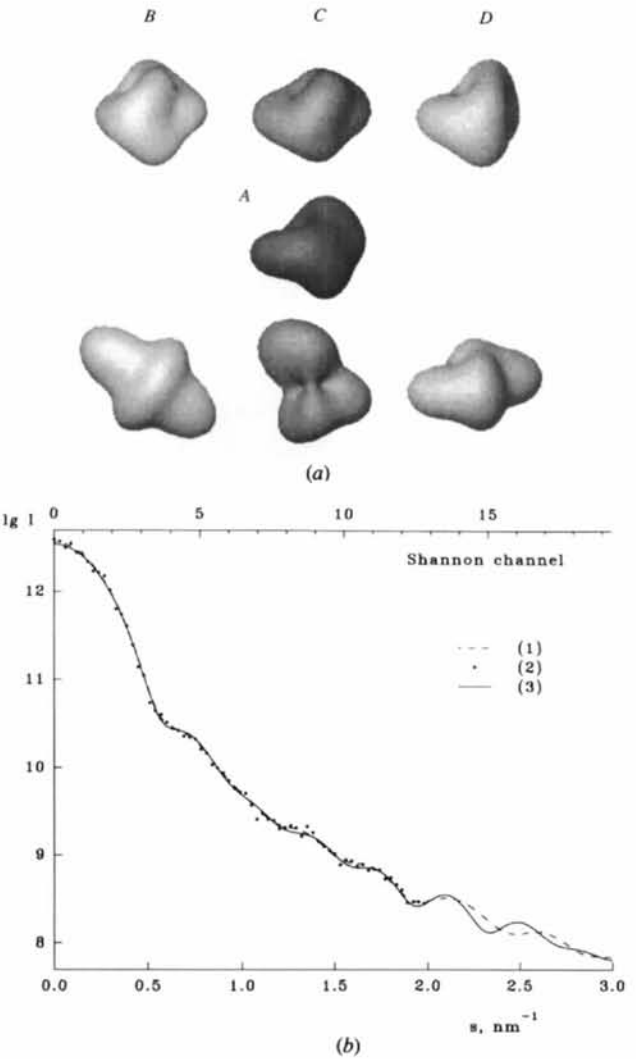

Fig. 5. Model-shape determination for $L = 4$ in the presence of random errors using the same angular ranges as in Fig. 3. (*a*) Model shape and its restorations (notations are the same as in Fig. 3*a*). (*b*) (1) ideal scattering from model *A*; (2) the same curve with 10% relative noise added; (3) scattering from the restored body *D*, top row.

Shannon channels [the estimation of the computational errors followed the finite-differences-table scheme of Hamming (1962)]. The error grows exponentially with s because the amplitudes $A_{lm}(s)$ are evaluated by the power series (5), which tends to diverge as the argument increases. The range of acceptable accuracy ($\delta I/I < 10^{-6}$ covers $N_s = 15$–17 Shannon channels; beyond this interval, the numerical errors worsen the results of any non-linear minimization procedure.

Better accuracy at higher angles is provided by the numerical integration

$$A_{lm}(s) = i^l(2/\pi)^{1/2} \int_{\omega} Y_{lm}(\omega)\, \mathrm{d}\omega \int_{0}^{F(\omega)} j_l(sr) r^2\, \mathrm{d}r. \quad (10)$$

As seen from Fig. 7, the numerical errors in this case do not significantly increase with s and the use of (10) becomes superior beyond the 15th Shannon channel. Numerical integration, however, is a time-consuming procedure and would lead to extremely large computing times to minimize (8).

Accumulation of the numerical errors imposes a resolution limit for the straightforward shape determination by restricting the number of model parameters that can simultaneously be refined. This is best illustrated in Fig. 8 where the three model bodies in Fig. 8(a) are each described by 30 independent parameters ($L = 5$) and display similar gross features but differ in finer details. The corresponding scattering curves in Fig. 8(b) differ by less than $R_I = 10^{-6}$ in the range $0 < s < 2\,\mathrm{nm}^{-1}$ (13 Shannon channels). In fact, shapes A and C were restored from the exact scattering curve of shape B in this interval starting from different initial approximations. Theoretically, as the curves differ for $s > 2\,\mathrm{nm}^{-1}$, the use of a wider angular range in the shape determination should have improved the solution. Practically, the computational errors at higher angles deteriorate the search direction so that further minimization becomes

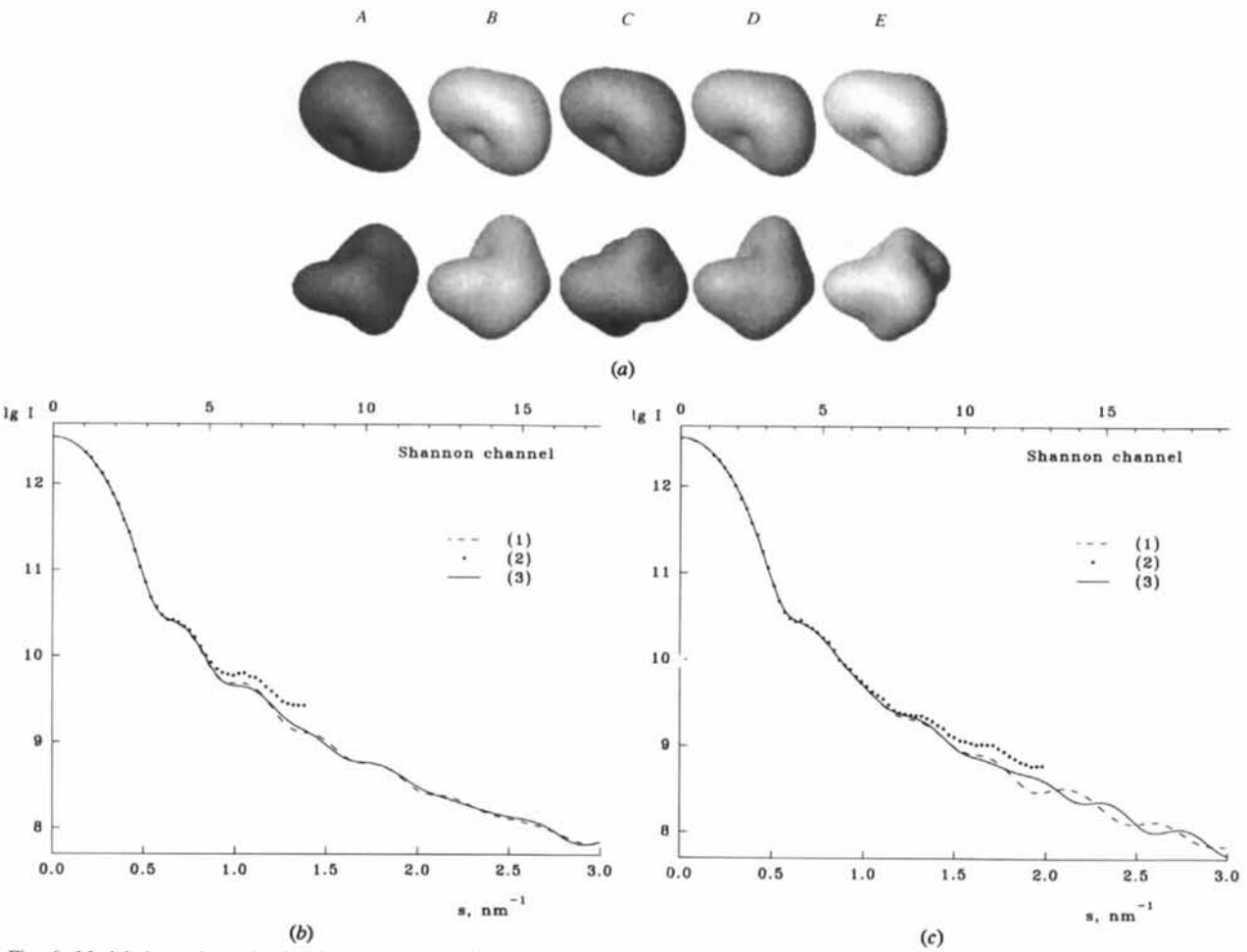

Fig. 6. Model-shape determination in quasi-real conditions. (a) Initial model (column A) and its restorations starting from different initial approximations (columns B–E). Top row: $L = 3$; bottom row: $L = 4$. (b) and (c) Scattering curves: (1) ideal scattering from the initial models; (2) the same curves with 3% relative noise and the constants added; (3) scattering from the restored bodies from column B.

impossible. Actually, the power-series representation (5) diverges beyond $s = 3.7\,\text{nm}^{-1}$ and the curves in Fig. 8 were evaluated using the direct integration (10).

6. Discussion

The model calculations performed in this study strongly suggest that the low-resolution shape determination for the error-free data is unique. Using the models based on envelope functions represented with spherical harmonics, it was not possible to find two different shapes at the same resolution (that is at the same L) that produce *exactly* the same scattering curve. In particular, the example in Fig. 8 indicates that the outer parts of the scattering curves do contain information about the finer details of the particle shape in contrast to the opinion (*e.g.* Taupin & Luzzati, 1982) that $I(s)$ beyond some scattering angle is fully described just by two parameters using Porod's law.

From the practical point of view, the most important conclusion is that the shape restoration is stable with respect both to termination effects and to experimental errors. In the presence of statistical errors, a reasonable shape restoration is achieved by fitting the portions of the scattering curves containing fewer Shannon channels N_s than the number of independent parameters in the model N_I ($N_I \cong 1.5N_s$). The reason is that data are oversampled (see *Introduction*) and the problem is non-linear, that is, the f_{lm} coefficients produce correlated contributions to $I(s)$. For a simple system of linear equations, the condition $N_I > N_s$ would degenerate the problem allowing a manifold of totally different solutions. For shape determination, it worsens the accuracy of the restoration but preserves the main features. Of course, by lowering N_s too much, quantity is transformed into quality and one may arrive at a completely different shape as shown in Fig. 5(*a*).

The spherical harmonics represent a full set of orthogonal functions and thus any envelope function $F(\omega)$ can be represented with their linear combination. The quality of this representation is improved with the resolution but the gross features of the particle are adequately described already at low multipole orders ($L \cong 4$). Therefore, the above results demonstrating the potential and limitations of the shape restoration in terms of spherical harmonics form a basis for an *ab initio* shape determination from the SAS data.

The limitations on the number of parameters that can simultaneously be determined do not mean that the structures with $L > 4$ cannot be reconstructed. If lower-order harmonics are known and fixed, the refinement of the higher-order coefficients is straightforward. In our model calculations (not shown) using the range over 13 Shannon channels, all 15 f_{lm} coefficients of the seventh

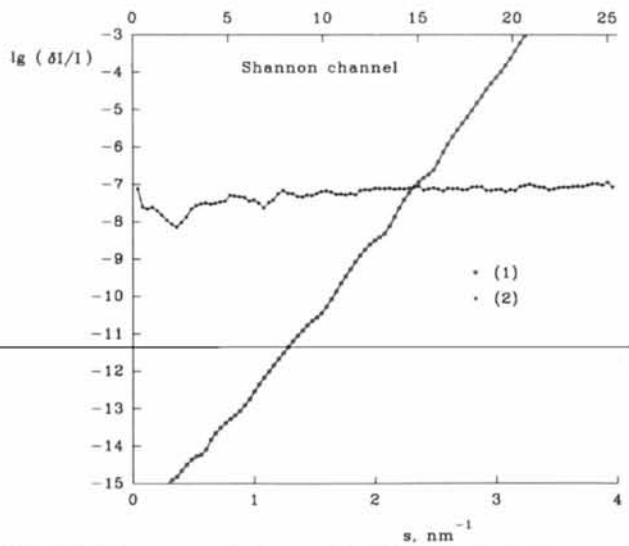

Fig. 7. Relative computational errors for different methods of evaluating $I(s)$: (1) using power series (5); (2) using numerical integration (10).

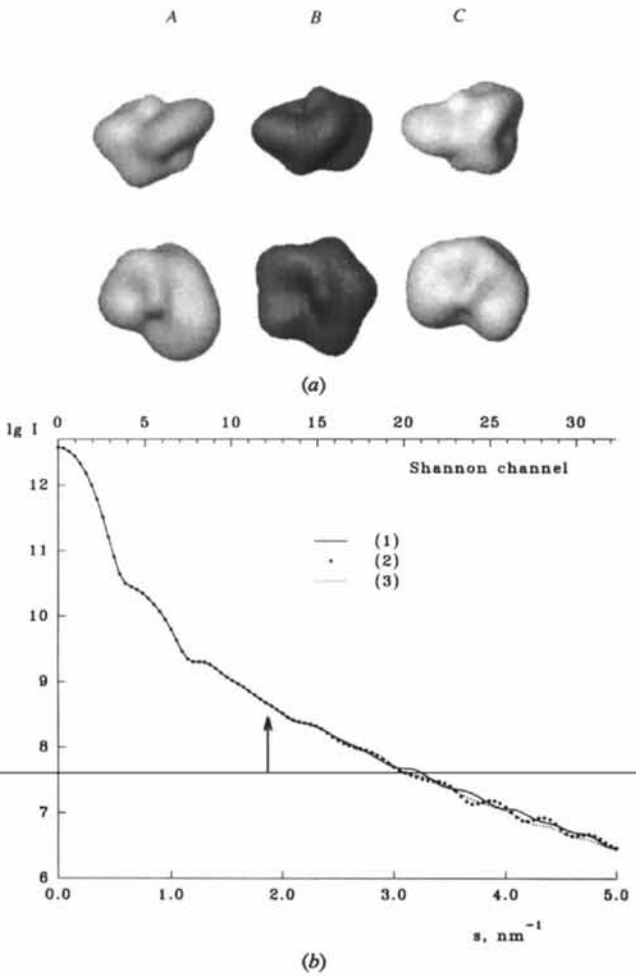

Fig. 8. Ambiguity at $L = 5$: (*a*) three bodies (*A*–*C*) in two different orientations (top and bottom rows). (*b*) Corresponding scattering curves (1)–(3). For explanations see text.

order are readily restored provided the coefficients from $l = 0$ to $l = 6$ are known. One can therefore improve the resolution using a chain refinement by taking into account more harmonics in series (2) and extending the fitting range.

As the present paper deals with the uniqueness of the shape restoration in principle, the model calculations were restricted to the ideal case, namely, to the envelopes with sharp boundaries exactly described by the limited number of spherical harmonics. In practical applications, deviations from the ideal model [*e.g.* finite width of the particle–solvent interface, truncation effects in the representation (2)] should be taken into account. Practical aspects of the shape determination and the details of our program package will be presented in a forthcoming paper.

The work was supported by NATO Linkage Grant LG 921231, INTAS Grant no. 93-645, by an EMBL fellowship to MBK and by a DAAD fellowship to VVV. The authors are indebted to M. H. J. Koch for useful discussions and to F. Golding for valuable comments on the manuscript.

References

Dennis, J., Gay, D. & Welsch, R. (1981). *ACM Trans. Math. Soft.* **7**, 348–368, 369–383.

Feigin, L. A. & Svergun, D. I. (1987). *Structure Analysis by Small-Angle X-ray and Neutron Scattering.* New York: Plenum Press.

Gill, P. E., Murray, W. & Wright, M. H. (1981). *Practical Optimization.* London: Academic Press.

Hamming, R. W. (1962). *Numerical Methods for Scientists and Engineers.* New York: McGraw-Hill.

Hunt, B. R. (1994). *Int. J. Mod. Phys.* **C5**, 151–178.

Koch, M. H. J. (1991). *Handbook on Synchrotron Radiation*, edited by E. Ebashi, M. Koch & E. Rubenstein, pp. 241–268. Amsterdam: North Holland.

Moore, P. B. (1980). *J. Appl. Cryst.* **13**, 168–175.

Shannon, C. E. & Weaver, W. (1949). *The Mathematical Theory of Communication.* Urbana: University of Illinois Press.

Stuhrmann, H. B. (1970*a*). *Acta Cryst.* A**26**, 297–306.

Stuhrmann, H. B. (1970*b*). *Z. Phys. Chem. (Frankfurt am Main)*, **72**, 177–184, 185–198.

Svergun, D. I. (1994). *Acta Cryst.* A**50**, 391–402.

Svergun, D. I. & Stuhrmann, H. B. (1991). *Acta Cryst.* A**47**, 736–744.

Taupin, D. & Luzzati, V. (1982). *J. Appl. Cryst.* **15**, 289–300.